Bioinspiration & Biomimetics

PAPER

Comparing the turn performance of different motor control schemes in multilink fish-inspired robots

To cite this article: Stephen P Howe *et al* 2021 *Bioinspir. Biomim.* **16** 036010

Bioinspiration & Biomimetics

PAPER

Comparing the turn performance of different motor control schemes in multilink fish-inspired robots

Stephen P Howe*, Andrew R Duff and Henry C Astley

University of Akron, Akron Ohio, United States of America
* Author to whom any correspondence should be addressed.

E-mail: stephen.p.howe@outlook.com

RECEIVED
12 August 2020

REVISED
4 January 2021

ACCEPTED FOR PUBLICATION
18 February 2021

PUBLISHED
12 April 2021

Keywords: robot, swimming, fish, control

Supplementary material for this article is available online

Abstract

Fish robots have many possible applications in exploration, industry, research, and continue to increase in design complexity, control, and the behaviors they can complete. Maneuverability is an important metric of fish robot performance, with several strategies being implemented. By far the most common control scheme for fish robot maneuvers is an offset control scheme, wherein the robot's steady swimming is controlled by sinusoidal function and turns are generated biasing bending to one side or another. An early bio-inspired turn control scheme is based on the C-start escape response observed in live fish. We developed a control scheme that is based on the kinematics of routine maneuvers in live fish that we call the 'pulse', which is a pattern of increasing and decreasing curvature that propagates down the body. This pattern of curvature is consistent across a wide range of turn types and can be described with a limited number of variables. We compared the performance of turns using each of these three control schemes across a range of durations and bending amplitudes. We found that C-start and offset turns had the highest heading changes for a given set of inputs, whereas the bio-inspired pulse turns had the highest linear accelerations for a given set of inputs. However, pulses shift the conceptualization of swimming away from it being a continuous behavior towards it being an intermittent behavior that is built by combining individual bending events. Our bio-inspired pulse control scheme has the potential to increase the behavioral flexibility of bio-inspired robotic fish and solve some of the problems associated with integrating different swimming behaviors, despite lower maximal turning performance.

1. Introduction

Complex, natural environments are difficult for conventionally designed robots and vehicles to navigate, leading engineers look to biology to inspire locomotor solutions. Limbed and limbless terrestrial robots can handle complex terrain that is difficult for conventional wheeled or tracked robots. As the use of remotely operated vehicles and autonomous underwater vehicles increases (especially in and around complex underwater structures) there is more interest in understanding the locomotor strategies of aquatic organisms. In certain cases, undulatory swimmers can be faster, more efficient, more maneuverable, and quieter (Fish 2013). Fish also have a diversity of propulsive systems that are tailored to different locomotor needs. The needs of remotely operated vehicles and autonomous underwater vehicles are similarly variable and as such the diversity of fish has translated to a diversity of fish robots (Anderson and Chhabra 2002, Blevins and Lauder 2013, Epstein *et al* 2005, Neveln *et al* 2013, Niu and Xu 2014, Wu *et al* 2015).

The best studied fish inspired robotic system is the laterally undulating robot (Cen and Erturk 2013, Jian-Xin and Xue-Lei 2011, Yu *et al* 2003, Ren *et al* 2012, Su *et al* 2014, Tomie *et al* 2005, Wang *et al* 2014, Xie *et al* 2020, Yu *et al* 2006, 2008, 2007, 2009, Yuan *et al* 2015, Zhang *et al* 2016, Yang *et al* 2018), though other systems exist (Blevins and Lauder 2013, Epstein *et al* 2005, Ming *et al* 2014, Neveln *et al* 2013, Yu *et al* 2016). Since Hirata *et al* (2000), fish inspired robots explore different sizes (Chen *et al* 2018, Phamduy *et al*

2017, Yu *et al* 2018), increased the number of segments (Bal *et al* 2019, Chen *et al* 2019, Su *et al* 2014, Wang *et al* 2014, Wu *et al* 2015, Yu *et al* 2008, Yu and Tan 2020), and explored different actuator technologies (Chen *et al* 2018, Coral *et al* 2018, Ming *et al* 2013, Zhong *et al* 2017, Zhong *et al* 2018). There are two general approaches to achieve turning in an undulating fish robot: the offset and the C-start. The offset turn involves biasing the bending of the body to the left or right (figures 1(A) and (B)). This is done by offsetting the waveform and can persist multiple swimming cycles. Offset turns do not fundamentally change the kinematics of the underlying swimming wave, e.g. amplitude or frequency, other than to bias it to the left or right. Several studies that utilize offset turns use biological reference points to validate kinematics. Ozmen Koca *et al* (2018) took detailed kinematic measurements of carp swimming to set the dimensions and behavior of their model robot. They used artificial intelligence to identify the link lengths and joint centers of a swimming carp and were able to find the oscillation frequency of each joint angle, to be used in their robotic model (Ozmen Koca *et al* 2018). Behaviors that resemble sequential offset turns are observed in live fish (Webb and Fairchild 2001, Howe and Astley 2020). The C-start takes its inspiration from escape maneuvers in live fish wherein steady swimming is interrupted and all the segments bend to one side before returning to their natural position (figures 1(C) and (D)). These mechanisms are rooted in muscle activation patterns observed in fish executing fast turns (Jayne and Lauder 1993). In single motor robots these maneuvers take the form of a constant deflection to one side where the tail acts a rudder (Hirata *et al* 2000, Tomie *et al* 2005). In multi-joint fish robots all motors can be activated at once to achieve the bent C shape, and then sequentially unbent from head to tail to return to a resting posture (Su *et al* 2014). C-start kinematics have also been approximated by fitting the joint centers to a circle that changes diameter and position relative to the body over the duration of the turn, thereby controlling the joint angles and propagating the wave behavior down the body (Jindong and Huosheng 2005). While innovative, this method of control has not been adopted in later studies.

Many recent robotic models utilize central pattern generators (CPGs) to control locomotion which allows the robot to integrate feedback and react to its environment as opposed to being completely feed forward (Bal *et al* 2019, Wang *et al* 2019, Wang *et al* 2014, Wang *et al* 2011, Wang *et al* 2013, Xie *et al* 2019, Yang *et al* 2018, Yu *et al* 2018, Yuan *et al* 2015). CPGs have several benefits for controlling fish robots: they are robust to disturbance, can integrate sensor feed back which allow the robot to respond to its environment, and can execute maneuvers outside the general undulating pattern (Ijspeert 2008). In order to interrupt a swimming wave to execute a high intensity turn like a C-start, the normal swimming wave must be suppressed or over-ridden. The control scheme must have a separate set of code designed to smoothly transition the body from a bent or straight posture as it hands control back to the steady swimming function (Su *et al* 2011). Otherwise, there is a discontinuity associated with starting a wave from a straight body position. This creates a 'jerky' motion that can place high stresses on motors (especially toward the tail) that often are transitioning to high motor angles. Due to their integrative response to error, CPGs can smooth out transitions between steady swimming and other behaviors like turns and glides (Xie *et al* 2019). Most CPG controlled robots use amplitude offsets to control turns (Bal *et al* 2019, Wang *et al* 2014, Wang *et al* 2011, Xie *et al* 2019). Xie *et al* (2019) validated the turn kinematics of a wire-driven robot with video taken from a live carp. In their CPG driven system, they were able to transition between steady swimming, turning, and gliding behaviors (Xie *et al* 2019).

In general, robotic fish implement swimming as a continuous behavior that can be described with periodic functions. Even when behaviors like gliding and fast turning are considered, they are considered additions to the otherwise continuous system. In biological fish, swimming is often intermittent (Ellerby *et al* 2018). Even when steadily swimming, fish are constantly adjusting course and dealing with obstacles. The kinematics of steady swimming across large groups of fish are very different to the turn kinematics we observed in live fish (Lauder *et al* 2018, Howe and Astley 2020). Steady swimming is characterized by low amplitude bending that is localized toward the tail end of the fish (Lauder *et al* 2018). This minimizes losses due to drag and increases efficiency (Borazjani and Sotiropoulos 2010). Turning often involves higher body curvatures that are started further up the body than steady swimming tail beats (Lauder *et al* 2018). The body of robotic control literature shows that it is possible to turn a fish by simply biasing the swimming wave to the right or left, but turning performance may be improved by including kinematic features observed in live fish swimming. In studying a wide range of routine maneuvers in live fish, we identified a kinematic pattern that has yet to be implemented in the fish robots. Turns can be modeled as sinusoidal peaks of bending that grow and shrink as the center of the peak propagates down the body (Howe and Astley 2020) (figure 1(A)). Importantly, the propagation of the center of the curvature peak happens immediately upon the initiation of the turn. Another feature is the initiation of bending around the mid-point of the body. Bending increases both anteriorly and posteriorly in live fish routine maneuvers during the first stage of the turn, and then the body segments begin to unfurl, propagating posteriorly as the turn completes during the second stage. We developed a turning mechanism based on our

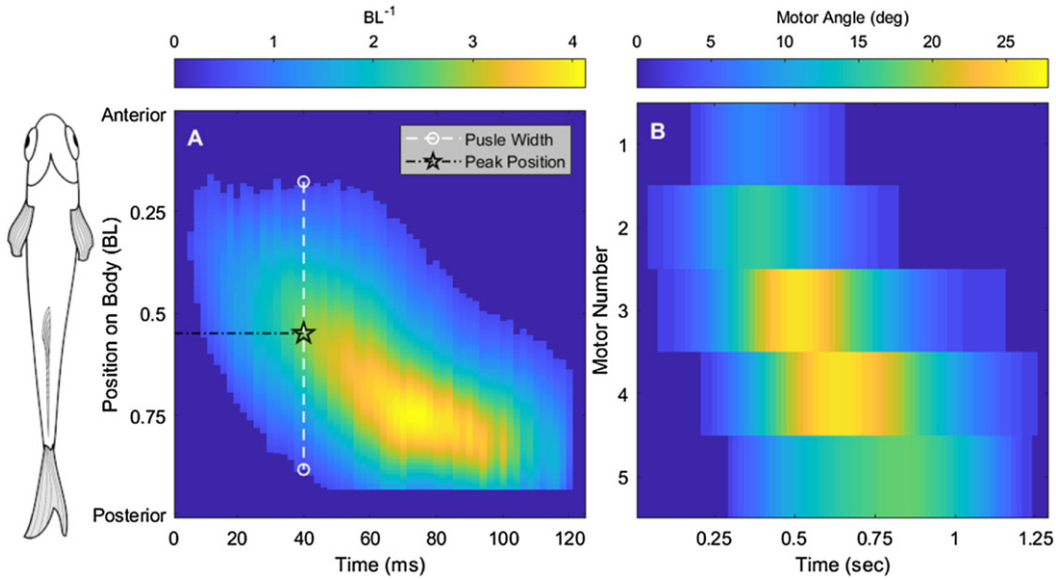

Figure 1. (A) Heat map of the curvature of the midline of a Giant Danio over the duration of a turn, described as a 'bending pulse' in Howe and Astley (2020). (B) Heat map of measured motor angle in bio-inspired pulse control scheme based on fish turns observed in Howe and Astley (2020). [Howe, S. P., & Astley, H. C.] John Wiley & Sons.

observations of routine turns in live fish that generalizes the patterns of deformation into a form that can be scaled to different commanded parameters. We will test the turning performance of our new routine-turn inspired control scheme against versions of existing robotic turning strategies. To our knowledge, this represents the first time different turning mechanisms are compared using the same multi-link robotic platform. While comparisons between control strategies could be made using meta-analyses from the existing literature, testing within the same robotic platform eliminates error that would be introduced from different equipment and design choices, such as robot shape, number of links, or motor choice. We predict that our new bio-inspired turn mechanism will perform better than the other control schemes we test, the offset and the bio-inspired C-start.

2. Methods

2.1. Robot construction

The actuated backbone of the robot consists of five waterproof servos (Hitec HS-5086WP, max torque: 0.3 N m, stall current draw 1800 mA) connected with custom 3D printed brackets. The Arduino Uno (Arduino Inc. Turin Italy) we used to control the robot can normally support five pulse width modulated channels and still have room for sensor input. Ozmen Koca *et al* (2018) and Akanyeti and Fetherstonhaugh (2020) found that most fish swimming kinematics could be sufficiently replicated with five or six segments. Simulations of sandfish swimming showed that the forces the sandfish exerts on the sand can be modeled with a reduced number of segments (seven in a robot, 14 in a simulation) (Maladen *et al* 2011).

The body shells were designed based on a profile image of a Giant Danio (*Devario aquepinnatus*, (McClelland 1839)) and was manually scaled to fit around the motorized backbone (figure 2). All 3D printed parts were designed in Autodesk Fusion 360 (Autodesk Inc. San Francisco California). A free-form t-spline surface was fit to the outline of the fish, excluding median fins. The dimensions of the robot are 493 mm long, 145 mm dorsoventrally, and 95 mm laterally. This body envelope was subdivided into six segments, thickened, and struts were designed to connect the shell to its corresponding motor bracket. The head was the longest body segment at 30% of the total length. The head in the robot is longer than the head we measured in live fish, but the amount of curvature we measured in this region on the fish's midline was low (figure 1(A), Howe and Astley (2020)). Active segments were the same length at 14% TL. A 45 degree wedge was cut from each side of the segment to allow for bending. Ports were designed to allow access to fasteners and to rout cables. All 3D printed parts were printed with ABS filament at 100% infill (figure 2). Buoyancy was controlled with floats and ballast affixed to various parts of the robot shells, which provided passive roll stability. To allow for fine scale buoyancy control, a 'swim bladder' was designed that consisted of a balloon, surgical tubing, a large syringe, and zip ties, and fit in the empty space in the dorsal portion of the third segment (figure 2(C)). We could manually adjust the amount of air in the swim bladder to allow for buoyancy adjustments during trials. The tail of the robot was constructed from two 0.5 mm mylar sheets secured with bolts in the base of the tail. A Lycra® skin was hand tailored to fit the shape of the robot (figure 2(D)). This was not intended to keep water out of the robot, but to reduce

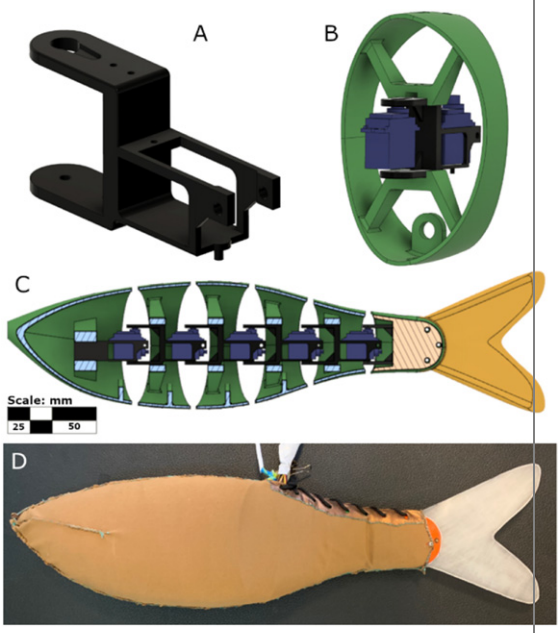

Figure 2. Schematic of robot construction. (A) Motor bracket (B) body segment consisting of a motor, bracket and body shell (C) cross sectional view of entire robot. (D) Robot with Lycra® skin. The scale bar is valid for (C) and (D), the entire bar is 100 mm.

flow in the inter-segmental spaces, which dramatically increased the speed of the robot. The servo wires were extended to allow us to use a larger testing area and still have access to power. The servos were connected to an Arduino with a custom servo shield. We used a Mastech HY-3020E DC power supply. Amperage was set to unlimited draw, voltage was set at 6 V (the maximum rating for the servos we used).

3. Design of turn mechanisms

We used three different turn mechanisms, two based on previous literature and one based on routine turning behavior we observed in live fish (Howe and Astley 2020). A trial consists of a steady swimming phase (3 tail beats), a coasting phase, the turn, and a final coasting phase. The steady swimming allowed the robot to start a turn at a moderate velocity (mean: 0.21 BL s^{-1}, s.d. 0.04), hence the steady swimming, but start from and return to a straight posture, hence the glide phases.

The first two control schemes drive steady swimming with a sinusoid that has a parabolic amplitude envelope based on equations derived by Lighthill (1960), with amplitude envelope coefficients adapted from Borazjani and Sotiropoulos (2010). This results in small head deflections, limited to no mid-body deflections, and exponentially wider tail deflections. Two of the coefficients were increased by a factor of ten as the original equations were based on the kinematics of mackerel swimming and were too fine to produce effective swimming. Increasing these coefficients increased the tailbeat amplitude slightly and allowed for a slow but effective swimming speed.

The offset control scheme is the simplest and is based on Hirata *et al* (2000), in which the turns of fish robots were controlled by adding an amplitude offset to the sine wave driving steady swimming. This offset caused a bias in the excursion of the tail to the left or right. The frequency and amplitude of the wave was unaltered. This mode of turning has been adapted in many other experiments (Clark *et al* 2012, Jian-Xin and Xue-Lei 2011, Kelasidi *et al* 2014, Morgansen *et al* 2007). These prior papers used single link robots whereas we are using a multi-link robot (figure 2). We decided to apply the same offset to the entire motor train (figures 3(A) and (B), supplemental video 1 (https://stacks.iop.org/BB/16/036010/mmedia)). This meant that the magnitude relative to the maximum angular excursion changed along the length of the robot; thus at very high offsets the anterior motors did not exhibit any contralateral bending.

The C-start control scheme is based on an approximation of escape response behavior in fishes and has been adapted to various robots (Hirata *et al* 2000, Su *et al* 2011). In this case all the motors simultaneously bend to the desired amplitude (figures 3(C) and (D)). In single link robots there is no need for a propagating offset, however to be fair to the model we programmed the motors to offset sequentially propagating from head to tail, like the EMGs of real fish (Jayne and Lauder 1993). We chose to achieve this behavior by initiating the unfurling of the motors at the same time with different return rates (figure 3(C), supplemental video 1).

We designed a new control scheme that is based on midline kinematics of routine maneuvers in live fish (Howe and Astley 2020) (figures 1(E) and (F) and 2). We described the midline deformations of the fish as a pulse of curvature that changes shape as it propagates down the body (figure 1(A)). The defining parameters of a pulse are the duration of the behavior, the maximum curvature, and the width of the pulse (which corresponds to how many body segments are active) (figure 4). These three parameters change independently over the duration of the turn, which itself is a variable that can be changed. To model the growth and propagation of these peaks we fit sinusoidal peaks to three points, a rostral end point, a caudal endpoint and a maximum angle centered between the two. These peaks change width and amplitude as they propagate down the body. We used three functions to describe the change of the pulse width, position of the peak, and the amplitude of the peak (figure 4). These functions are unitized so they can be scaled to any combination of inputs. All three functions describe the change in their parameters with respect to time (t). The pulse is propagated by a peak transform function (figure 4(A)). In many turns, we observed that the peaks of the curvature pulses propagated nonlinearly (Howe and Astley 2020). When developing

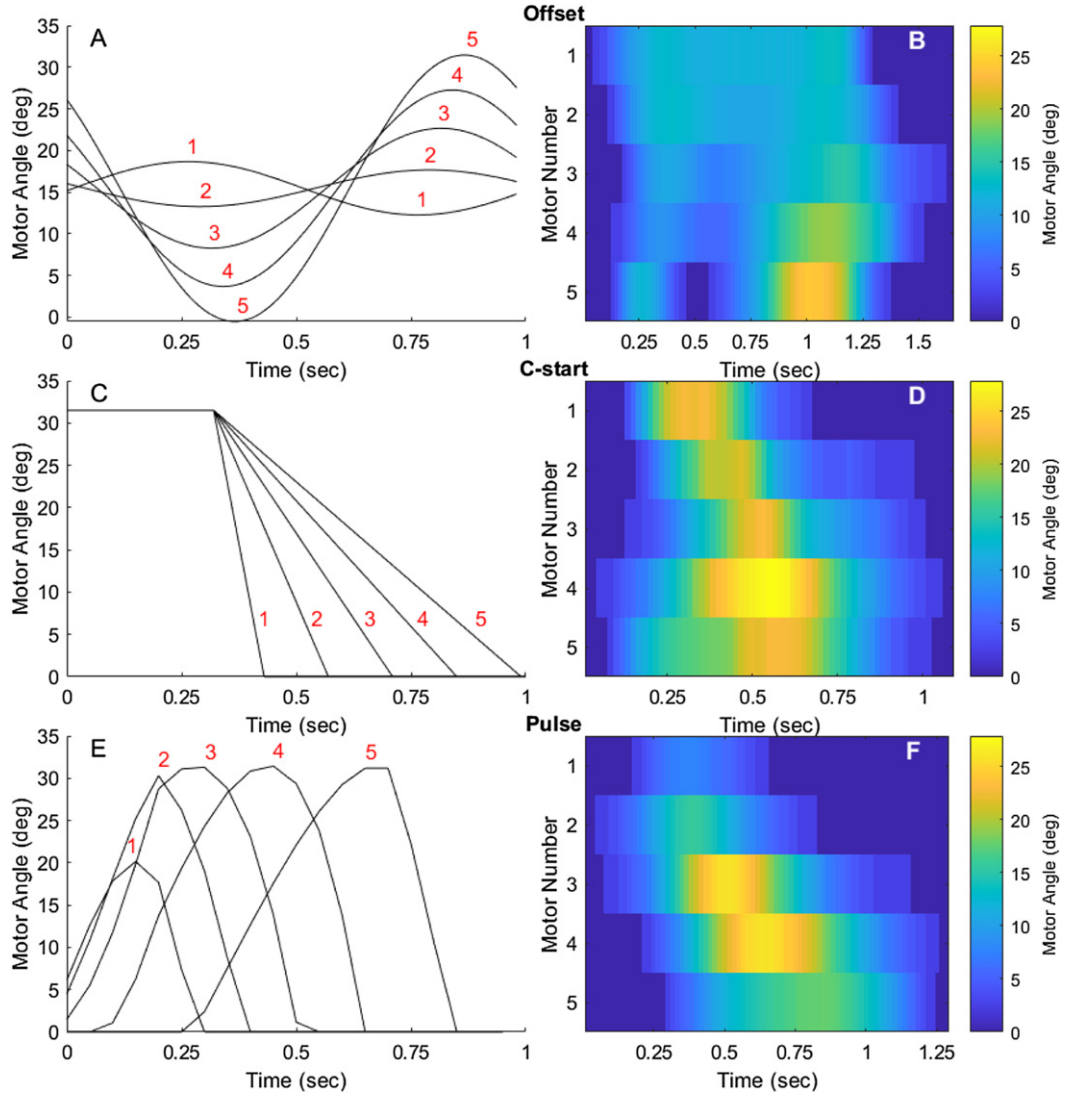

Figure 3. Side by side plots and heat maps of the commanded kinematics for each control scheme and their measured motor angles. In each of these examples the commanded duration was set to 1 s and the commanded angle was 31.5 deg. In subplots (A), (C) and (E) lines show the change in angle over time and each line is labeled according to its motor number. (A) and (B) Offsets (C) and (D) C-start (E) and (F) pulses.

the control scheme, we tested pulses with linear and parabolic propagation functions and found that the parabolic function performed better. At $t = 0$ the peak is centered at 0 (the head of the fish) and progresses to 1 (the tail of the robot) as $t \to 1$. This function is multiplied by the pulse origin, which we held constant at 26% BL for turns, thereby scaling the peak propagation behavior to the input origin and duration. In live fish the maximum curvature occurred at about 50% the pulse duration. We approximated this behavior with a symmetrical trapezoid function where amplitude (a), increases to $a = 1$ at $t = 0.25$, remains constant then begins to decrease back to $a = 0$ at $t = 0.75$ (figure 4(B)). In live fish the maximum width (w) occurs at approximately one third the pulse duration. We coded this behavior as a line starting at $w = 1$ at $t = 0$ and ending at $w = 0$ where $t = 1$ (figure 4(C)). We moved the maximum width earlier in the pulse, eliminating the ramp-up phase as it improved the behavior of the pulse, resulting in the line that decreases from 1 to 0 with unit slope. When combined with the other functions, this produced a motion similar to the biological fish (figure 1). The maximum pulse width was held constant for the turns we tested at 1 body length. At a given time (t) the code reads its position on each of these functions to determine the center, ends, and peak of the sinusoid pulse. A sinusoidal peak is fit to these three points (figure 4(D)). The motors that fall within the bounds of the peak read the angle they are supposed to achieve. This process repeats for the duration of the pulse (supplemental video 1). Several of these functions and values do not exactly match the values and functions from the live fish they are based on, but they are consistent with the general patterns of body deformation we observed in live fish. We chose values that resulted in measured

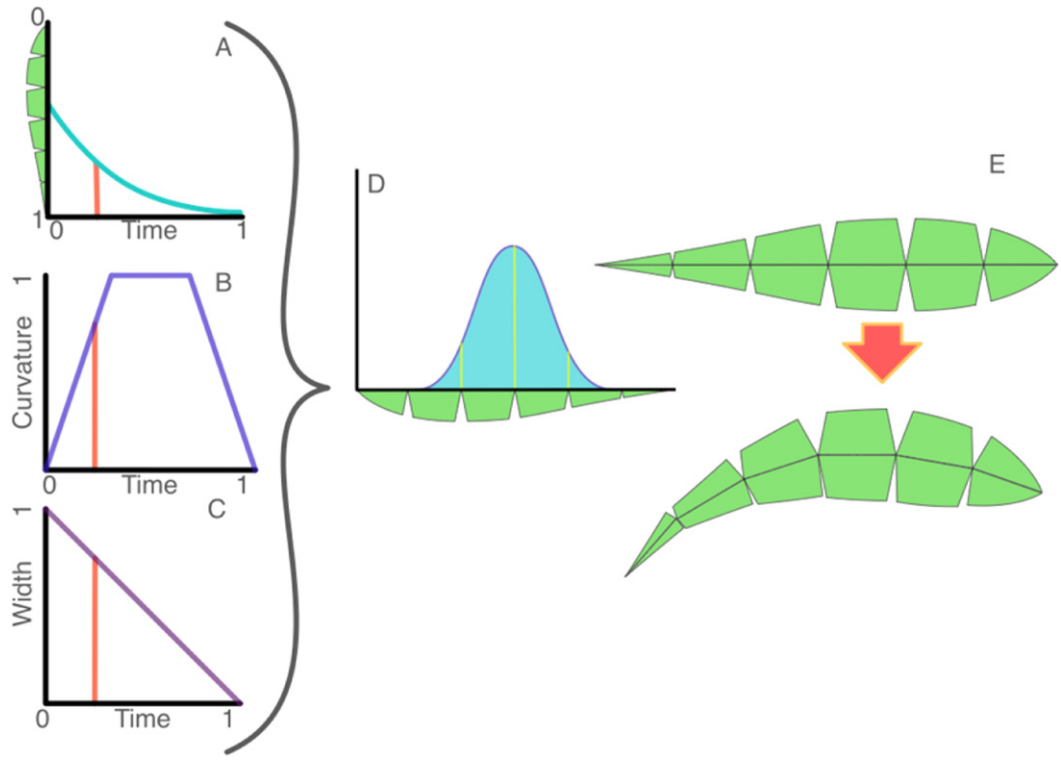

Figure 4. Schematic of the Pulse control scheme. (A) The peak propagation function. (B) The amplitude function (C) the width function (D) the fitted sine pulse at the given time (t) (E) comparison between a straight posture and the resulting bent posture. The vertical lines in (A)–(C) indicate the values of each function at time (t).

Table 1. Range, means, and standard deviations for turn duration and maximum summed angle across control schemes. Different letters indicate significant differences between means. The control schemes are C-starts (CS), offsets (OF), and pulse turns (PT).

	CONTROL SCHEME	MINIMUM	MEAN	S.D	MAXIMUM	PAIRWISE
TURN DURATION (SEC)	CS	0.7	1.31	0.42	2.08	A
	OF	0.58	1.79	0.58	2.8	B
	PT	0.7	1.92	0.79	3.41	C
MAXIMUM SUMMED ANGLE (DEG)	CS	42	86	23	143	A
	OF	18	74	31	133	B
	PT	34	68	20	106	C

kinematics in the robot that better matched the kinematics in the live fish. Optimization of these commanded parameters would likely improve the robot's performance.

Multiple pulses can be combined to achieve steady swimming and complex behaviors using a 'digital punch card' which is a string of characters consisting of breaks (B), turns (T), and steady swimming (S). These letters are arranged in groups that reflect the set duration of the behavior. There are two 'punch cards' simulating right and left banks of muscles, the code reads the letters from each string and selects the corresponding set of input values. The motor positions are calculated independently for each side and summed to find the net motor angle. The breaks are spacers that can allow the robot to glide or change the amount of co-activation between the punch cards. This allows multiple pulses to be combined alternating left and right to achieve steady swimming. Using this method, the robot had a similar initial velocity as the sinusoidally controlled control schemes (0.18 BL s^{-1}). The full Arduino code is available in the supplementary material.

3.1. Data collection

We swam the robot in the Ocaseck Natatorium, University of Akron, Akron Ohio, and a private outdoor pool. A GoPro Hero 6 (GoPro, San Mateo, California) was affixed to a tripod that was submerged approximately 2.5 m under water. This gave us the field of view (3.5 × 5 m) we needed to track the robot through an entire turn. The camera recorded at 60 FPS and 1080P with the field of view set to linear. Each trial consisted of three straight swimming tail

Table 2. Table of means and standard errors for each center of mass outcome variable. Different letters indicate significant differences in means. The control schemes are C-starts (CS), offsets (OF), and pulse turns (PT).

D.F. 1,288	CONTROL SCHEME	MARGINAL MEAN	STD. ERR	TUKEY
TOTAL HEADING CHANGE (DEG)	CS	38.00	1.38	A
	OF	41.91	0.72	B
	PT	33.80	0.80	C
RECOIL (DEG)	CS	23.10	1.05	A
	OF	14.46	0.55	B
	PT	11.90	0.61	C
MEAN LINEAR ACCELERATION ($M \cdot SEC^{-2}$)	CS	-0.004	0.004	A
	OF	0.03	0.002	B
	PT	0.04	0.002	C
MAXIMUM CENTRIPETAL ACCELERATION ($M \cdot SEC^{-2}$)	CS	0.289	0.014	A
	OF	0.280	0.007	A
	PT	0.248	0.008	B

beat cycles followed by a single turn from a given setting. The robot was allowed to glide a short duration before it was reset to the starting position. One researcher was in the pool retrieving and resetting the robot after each trial, monitoring the progress of the trial to ensure the quality of the trial. A second researcher, above the water, manipulated the servo wires, attached to a PVC pipe, to avoid any pull or drag on the robot. The robot swam just beneath the surface of the water. We tested turns at half second intervals from a half second to 2 s for a total of four duration levels. We tested five amplitude levels that were fractions of the maximum angle (45°) (40%, 55%, 70%, 85%, 100%), which converts to 18°, 24.75°, 31.5°, 38.25° and 45°.

We used a custom written image analysis program discussed in detail in Howe and Astley (2020) (supplementary material), that reconstructs the midline of the robot, calculates the curvature along the midline, and tracks the centroid of the binarized image of the robot. The midlines are smoothed before curvature is calculated. Motor joint angles were calculated by estimating the position of the joint centers based on the splined backbone and the relative lengths of each body segment. To limit noise, we sampled joint angles that exceeded the threshold of 5% the maximum angle in the video, though this will cause the analysis to underestimate the absolute turn duration.

To verify the robot is performing as commanded, we measured several variables related to motor performance: the maximum individual motor angle, the observed turn duration, the maximum summed motor angle, and the ideal summed motor angle. Maximum motor angle is the maximum motor angle measured at any joint over the duration of the turn. Turn duration is the length of time between the first frame with a motor angle above the threshold to the last frame with the same. Summed motor angle is the sum of all motor angles on the robot during a given frame, maximum summed motor angle refers to the frame with the highest summed angle. Summed motor angle error is the ratio between the difference between observed maximum summed motor angle and the commanded maximum summed motor angle divided by the commanded maximum summed motor angle. We also computed the error between the commanded duration and the observed turn duration in the same way.

We measured the following variables corresponding to maneuverability and agility: total heading change, recoil, mean linear acceleration and maximum centripetal acceleration. Total heading change is heading of the robot upon entering the second glide phase minus the initial heading. Recoil is the difference between the maximum heading change and the final heading change (supplemental video 2). Linear and centripetal acceleration are the components of the acceleration vector of the centroid that are parallel and perpendicular to the velocity vector at a given time. Mean linear acceleration is the average linear acceleration over the duration of the turn. Maximum centripetal acceleration is the maximum instantaneous centripetal acceleration.

3.2. Statistics

All statistical analyses were conducted in JMP 14. We pruned our dataset down to five trials per turn setting (100 per control scheme, 300 total), selecting the five trials that had initial velocities nearest the global mean. Initial velocity was not a significant effect in any of the models, so it and its interaction terms were excluded from the model. The different turn control schemes have different commanded summed motor angles, across control schemes C-starts have

Table 3. Contains the coefficients of the control scheme*effect interactions between motor kinematics and total heading change, recoil, maximum centripetal acceleration, and mean linear acceleration. The value column denotes the slope of the interaction between the control scheme group and the effect. Bolded *p* values and different pairwise letters are significant after Bonferroni correction. The effects are input angle (IA) and input duration (ID). The control schemes are C-starts (CS), offsets (OF), and pulse turns (PT).

	INTERACTION	TEST	VALUE	STD ERROR	T RATIO	PROB>|T|	PAIRWISE
TOTAL HEADING CHANGE (DEG)	Achieved Total Angle (deg)	IA*CS=0	0.62	0.04	13.79	**<0.0001**	AB
		IA*OF=0	0.72	0.02	31.64	**<0.0001**	A
		IA*PT=0	0.56	0.04	14.40	**<0.0001**	B
	Pulse Duration (sec)	ID*CS=0	7.38	2.16	3.41	**<0.0001**	AB
		ID*OF=0	13.82	1.23	11.24	**<0.0001**	A
		ID*PT=0	7.27	0.95	7.62	**<0.0001**	B
	INTERACTION	TEST	VALUE	STD ERROR	T RATIO	PROB>|T|	PAIRWISE
RECOIL (DEG)	Achieved Total Angle (deg)	IA*CS=0	0.08	0.03	2.30	**0.02**	A
		IA*OF=0	0.21	0.02	12.25	**<0.0001**	B
		IA*PT=0	0.08	0.03	2.88	**0.004**	A
	Pulse Duration (sec)	ID*CS=0	20.14	1.63	12.33	**<0.0001**	A
		ID*OF=0	5.89	0.93	6.33	**<0.0001**	B
		ID*PT=0	3.81	0.72	5.28	**<0.0001**	B
	INTERACTION	TEST	VALUE	STD ERROR	T RATIO	PROB>|T|	PAIRWISE
MEAN LINEAR ACCELERATION	Achieved Total Angle (deg)	IA*CS=0	0.0005	0.0001	3.79	**<0.0001**	A
		IA*OF=0	0.0005	0.0001	8.36	**<0.0001**	A
		IA*PT=0	0.0007	0.0001	6.25	**<0.0001**	A
	Pulse Duration (sec)	ID*CS=0	-0.07	0.006	-11.20	**<0.0001**	A
		ID*OF=0	-0.03	0.003	-7.63	**<0.0001**	B
		ID*PT=0	-0.05	0.003	-18.66	**<0.0001**	A
	INTERACTION	TEST	VALUE	STD ERROR	T RATIO	PROB>|T|	PAIRWISE
MAXIMUM CENTRIPETAL	Achieved Total Angle (deg)	IA*CS=0	0.002	0.0005	4.84	**<0.0001**	A
		IA*OF=0	0.003	0.0002	11.08	**<0.0001**	A
		IA*PT=0	0.003	0.0004	7.99	**<0.0001**	A
	Pulse Duration (sec)	ID*CS=0	-0.17	0.02	-7.46	**<0.0001**	A
		ID*OF=0	-0.07	0.01	-5.49	**<0.0001**	B
		ID*PT=0	-0.12	0.01	-11.78	**<0.0001**	AB

a maximum summed motor angle of 5*X* the commanded angle, whereas pulses have a maximum of 2.8*X* the commanded angle, and offsets have a maximum summed angle that increases with increasing commanded angle. We also found considerable differences between the commanded parameters (angle and duration) and the measured kinematics. This error could have multiple sources and affects the overall statistical analysis. To ensure fair comparisons between the control schemes we constructed linear models testing, total heading change, recoil, and mean linear acceleration with the measured continuous variables (maximum motor angle and turn duration) as continuous effects, control scheme as a categorical effect, and their interaction terms, resulting in a total of four linear models, one for each outcome variable. In models where control scheme was a significant predictor, we conducted a Tukey's HSD test to test differences in means. In models with significant interactions between control scheme and a continuous predictor we tested the slope of the interaction against zero and the slopes of each of the control schemes. These tests were designed using the custom test feature in JMP, the coefficients for each test are provided in the supplemental materials. All interaction tests across the four linear models were collated and their significance was assessed using the Holm–Bonferroni correction.

4. Results

Over all types of maneuvers, the robot achieved maximum summed angles ranging from 143° to 17° with a mean of 76° (s.d. 26°). C-starts had the highest summed motor angles on average, followed by offsets and pulses, all significantly different from one another (table 1). Turn duration ranged from 3.4 s to 0.6 s with a mean of 1.7 s (s.d. 0.7 s). Pulses had the longest turn duration followed by offsets and finally C-starts (table 1) despite identical commanded durations. Across all control schemes, our robot completed turns ranging from 103° to 3° with a mean heading change of 39° (s.d. 21°). Mean heading change was not significantly different between offsets and C-starts but both were significantly higher than mean heading change in pulses (table 2). Recoil had an overall range of 0° to 42° with a mean recoil of 15° (s.d. 9°). C-starts had the

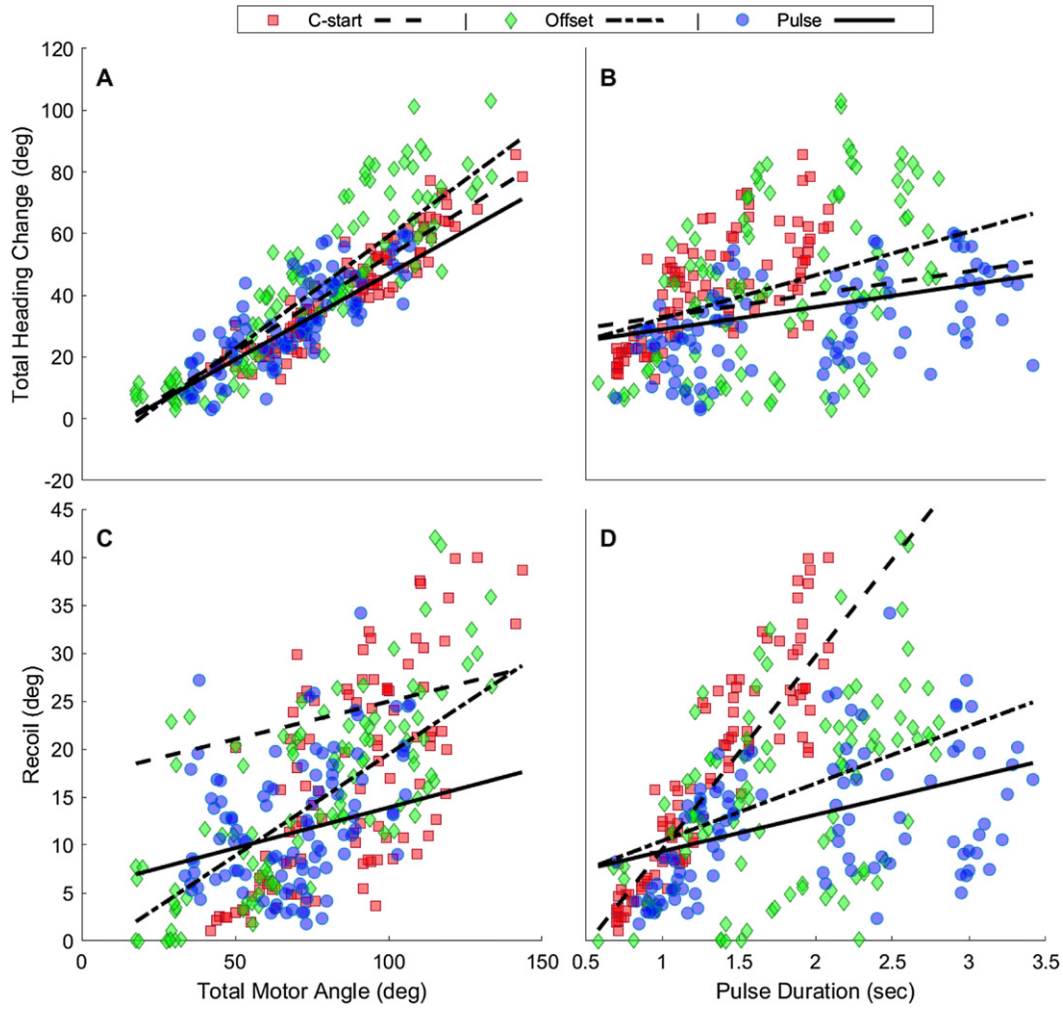

Figure 5. Plots of measured motor kinematics against total heading change and maximum centripetal acceleration. See table 2 for slopes and *p* values.

highest mean recoil followed by offsets and pulses; all pairs were significantly different (table 2). Mean linear acceleration had a global average of 0.02 m s^{-2} (s.d. 0.03). Mean linear acceleration was highest in pulses followed by offsets and C-starts, all pairs are significantly different (table 2). Maximum centripetal acceleration had a global range from 0.3 m s^{-2} to 0.6 m s^{-2} with a mean of 0.27 m s^{-2} (s.d. 0.13). C-starts and offsets had on average the highest maximum centripetal accelerations. They were not significantly different from one another, but both were significantly higher than pulses (table 2).

All four linear models were significant after Bonferroni correction (D.F. 1287; $p < 0.0001$). Summed motor angle had a significant effect on total heading change (table 3 and figure 5(A)). Though the interaction between summed motor angle and control scheme is significant, the differences in slopes is minimal. Turn duration also had a significant though much smaller effect on total heading change (table 3 and figure 3(B)). Recoil was the lowest in pulses, followed by offsets and then C-starts (table 3 and figure 5(C)). In pulses and C-starts summed motor angle did not have a significant effect on recoil, whereas in offsets summed motor angle had a significant positive effect on recoil, i.e. recoil increased with increasing summed motor angle. Turn duration had significant positive effects on recoil across all control schemes, though C-starts had the highest slope (table 3 and figure 5). Mean linear acceleration was highest in pulses followed by offsets and C-starts (table 3 and figure 6). Summed motor angle had a positive effect on mean linear acceleration across all control schemes that were all significantly different from one another (table 3 and figure 6(A)). Turn duration had a negative effect on mean linear acceleration. Pulses and C-starts did not have significantly different slopes, whereas offsets had a significantly shallower slope than the others (table 3 and figure 6(B)). The general relationships were similar for maximum centripetal acceleration. Summed motor angle had significant positive effects on maximum centripetal acceleration across all control schemes (table 3 and figure 6(C)), and turn duration had significant negative effects on maximum centripetal acceleration (table 3 and

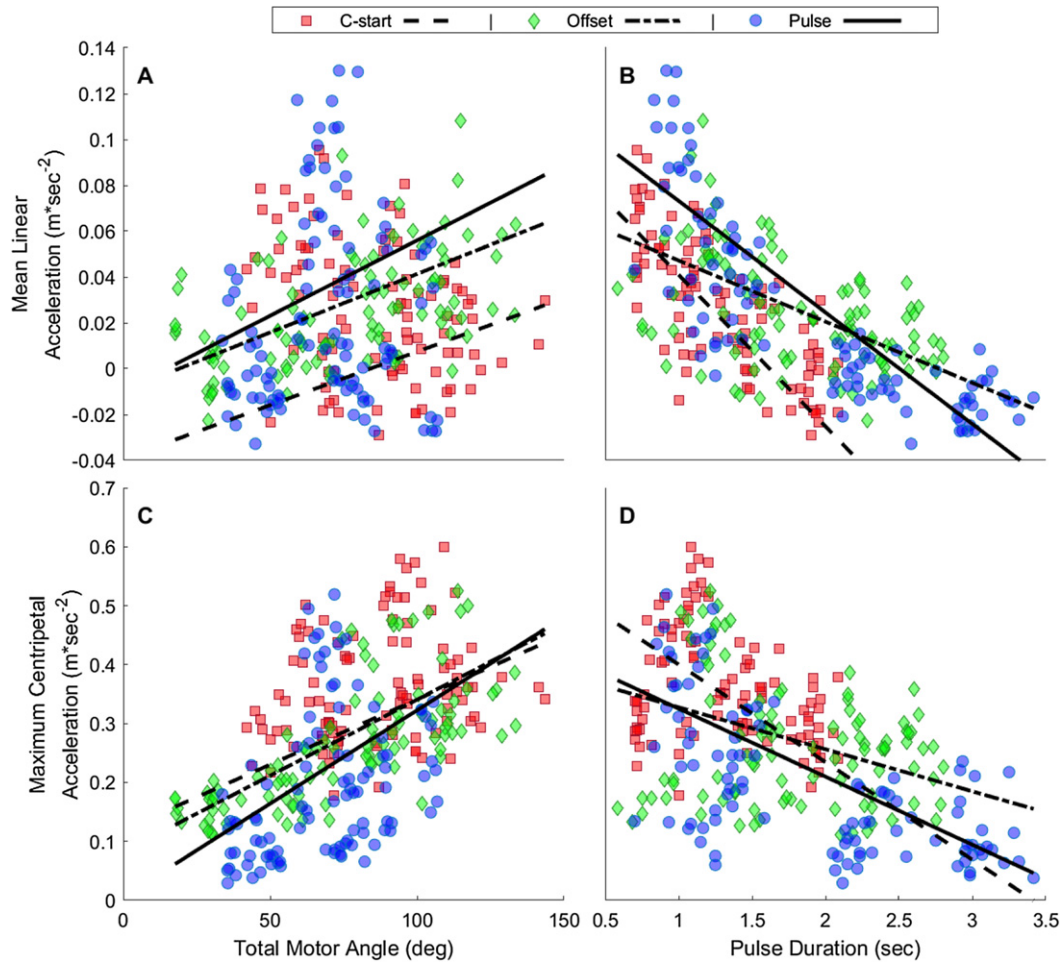

Figure 6. Plots of measured motor kinematics against mean linear acceleration and maximum centripetal acceleration. See table 2 for slopes and *p* values.

figure 6(D)). There was no significant interaction between maximum summed motor angle and maximum centripetal acceleration, i.e., the slopes were similar across control schemes. C-starts had a significantly steeper slope than offsets and pulses were not significantly different from either (table 3 and figure 6(D)).

5. Discussion

In this paper, we implemented a novel bio-inspired turn mechanism in a robotic model fish based on patterns of body deformation we observed in routine maneuvers of live fish (Howe and Astley 2020), and compared this new control scheme performed to existing turning methods for fish robots. We found that the performance relationships observed in the robot are generally consistent with those observed in live fish. Total body bending had significant positive effects on both total heading change and maximum centripetal acceleration in both systems (Howe and Astley 2020). Turn duration had a negative effect on acceleration, i.e., shorter turns are faster. We found that duration had a positive, though small, effect on total heading change in the robots, versus finding no significant relationship in live fish. These relationships were true in the robot regardless of turn control scheme. Generally, tighter body curvatures correspond to greater heading change and the faster the body-deformations are completed, the faster the turn. We expected the pulse control scheme to outperform C-starts and offsets. While pulses performed better in terms of mean linear acceleration and recoil, C-starts and offsets outperformed pulses in terms of heading change and maximum centripetal acceleration.

In fish, maximum overall curvature (the equivalent of summed motor angle), was a powerful predictor of turn outcomes, similarly, differences in summed motor angle in robot control schemes have strong effects on turn outcomes. C-starts are encoded with the highest potential summed motor angle (5*x* the commanded angle) across all commanded angles. Pulses similarly have a consistent, though much lower potential summed motor angle (2.85*x* commanded angle). However, in offsets the multiplier increases with increasing commanded angle. At the lowest commanded angle (18°) the potential summed angle is 0.85*x* commanded angle whereas at the highest commanded angle (45°) the potential summed angle is

3.34*x* the commanded angle. This is because as commanded angle increases, less of the body is involved in the contralateral undulation which takes away from the total body curvature. At the highest commanded angles, the motors do not cross the zero mark when completing the undulation cycle. In this way offsets become more like C-starts as commanded angle increases. When we control for the achieved summed motor angle and turn duration, we find that the performance differences between control schemes are less distinct. The relationship between summed motor angle and total heading change is very similar across control schemes. C-starts and offsets achieve higher summed motor angles overall and therefore achieve higher total heading changes. The slopes are significantly different, but the differences are small. It is likely that if we were to alter the pulse control scheme in a way that increased its potential summed motor angle, pulses would continue to increase in heading change alongside the other two control schemes. Our decision to use a uniform offset instead of a proportional offset (as in Pin *et al* (2011)), likely improved the performance of the offset turns. A proportional offset would have a much lower potential summed motor angle as the mid-segments of the body would not be allowed to bend as much as the uniform offset. While in most cases maximum angle is correlated with the intensity of the turn, summed angle provides a better view of the overall behavior of the robot. The bending of a single joint does not reveal as much about how far the robot or fish is deflecting its head as knowing the total curvature.

In this experiment we were unable to directly record measures of efficiency, like power consumption. However, recoil and mean linear acceleration offer insight into the relative efficiency of each of the turn control scheme. Recoil is the difference from the maximum heading change and the final heading change. Ideally recoil would be zero, and in live fish recoil is close to zero (Howe and Astley 2020, supplementary material). Pulses have the lowest recoil among all the control schemes, and had a significant, though small, increase with increasing achieved summed motor angle. C-starts also had a significant (but small) positive relationship between summed motor angle and recoil, whereas Offsets had a much stronger positive relationship, i.e. recoil increases with increasing summed motor angle. Recoil increases in all control schemes with increasing turn duration, but C-starts have a much steeper slope than pulses or offsets. Recoil represents energy lost trying to change the robots heading. Recoil continues to be a problem for fish robots (Xie *et al* 2020, Xie *et al* 2019). Xie *et al* (2019) commented on the lack of recoil in the carp they observed swimming, noting that the fish used its pectoral fins to eliminate recoil. Xie *et al* (2020) found that recoil could be reduced in steady swimming by changing the behavior of the tail beats, and that recoil and velocity trade off. Live fish have many more degrees of freedom to control the deformations of their body as well as auxiliary appendages like fins that likely work together to achieve turns with near zero recoil. Optimization of the kinematics of our model may reduce the amount of recoil, but we may be limited in how much recoil can be eliminated in a low degree-of-freedom system. Similarly, pulses have the highest mean linear accelerations of all control schemes tested, i.e., for a given summed angle or turn duration, pulses accelerate more. At higher durations, all control schemes slowed down over the course of the turn instead of speeding up. During a turn, the robot is balancing the drag associated with deforming its body with the thrust it can generate by accelerating water. At these high durations, the thrust is likely lower than the drag. Pulses have a higher intercept which indicates they may be better able to accelerate the water they gather during the turn, or pulses may experience less drag due to their body deformations or recoil. A combination of the two is likely but would require flow visualization experiments to confirm.

Despite the differences in programmed kinematics, C-starts exhibited some observed kinematics that caused them to resemble the outcome of the pulse control scheme in certain ways. If the motors had no resistance from the water and were able to move to their positions as expected, we would expect to see all the motor angles increase together and sequentially decrease. Instead, we see the motors all initiate bending at the same time but sequentially reach their maximum angles (figure 1(D)). This emergent behavior is similar to the propagating behavior that we observe in routine turns in live fish, which we replicated with our pulse mechanism. C-starts in live fish exhibit muscle activation patterns that are more akin to the C-start control scheme that we, and others (Jindong and Huosheng 2005, Su *et al* 2011, 2014), have encoded, wherein all the muscles activate simultaneously and deactivate sequentially (Jayne and Lauder 1993). However, in our observations of the kinematics of C-starts, we found that the patterns of developing and propagating curvature were similar regardless of the type of stimulus, though escape maneuvers were much higher intensity than routine maneuvers (Howe and Astley 2020). Interactions between the neuromuscular system, the material properties of the body, muscle physiology, and the forces imposed on the body by the water all likely work together to create the kinematic patterns we observe in live fish (Tytell *et al* 2011), it would make sense that combinations of similar factors could give rise to the kinematic patterns we observed in the C-start control scheme.

In this paper we compare the turning performance of three different methods of turning a fish robot. However, turning is one part of a whole system of swimming and must be integrated with other behaviors like steady swimming and gliding. There is an inherent problem combining a continuous sinusoidal swimming wave with behaviors and turns in that the

robot must be able to smoothly transition from a straight or bent posture to an S-shaped posture. In single actuator robots this can be achieved by introducing the turn or glide in phase with the swimming motion (Hirata *et al* 2000). In multi-link robots this becomes more difficult as there is a phase lag between the anterior and posterior motors. If one tried to transition the first motor into a new behavior at the same time as the last motor, the latter would be making large angular deflections to achieve its sinusoidal position, and this could require torques beyond the capabilities of the motor. Su *et al* (2011) worked on a method of integrating C-starts with steady swimming that sequentially transitioned the motors out of the C-start and back into steady swimming. This required a separate block of code to guide this transition (Su *et al* 2011). CPG-driven robots can more smoothly transition between behaviors (Xie *et al* 2019). However, most robots assume that a continuous steady sinusoidal gait is the natural state of the robot, and that glides and turns are behaviors that interrupt this swimming. Different fish will vary in their overall proportion of time spent swimming versus stationary, but steady swimming uninterrupted by obstacles or flow disturbances is the exception rather than the rule (Ellerby *et al* 2018). Even when fish maintain prolonged forward motion, it is often integrated with changes in course and corrections to disturbances. We suggest the opposite approach and treat the straight body posture as the natural state and behaviors like swimming or turning as departures from this state.

Modeling swimming as combinations of pulses has the potential to provide increased flexibility and opportunity to easily implement complex maneuvers required for these robots to navigate complex underwater environments. Our system of robot control is based around the pulse as the fundamental unit of swimming which can be combined to achieve complex behaviors. We observed fish building complex maneuvers from multiple pulses in series that could vary in amplitude and duration (Howe and Astley 2020). We can replicate some of these behaviors in the fish robot (supplementary video 3). In this system we treat steady swimming as a composite behavior consisting of equal strength left and right-handed pulses that overlap in time. We used this behavior to achieve the steady swimming immediately prior to the turn. These pulses have a more posterior pulse origin and lower amplitude than turning pulses, but the fundamental pattern of deformation is the same between the two behaviors. We were able to re-create the asymmetric tail beats observed in Webb and Fairchild (2001); behaviors that are the basis of offset models (supplementary video 3). In this case we combined higher amplitude turn pulses on one side with lower amplitude contralateral straight swimming pulses. We were not able to compare the efficiency of our model with the other bio-inspired control schemes over multiple pulses. That said, given the observed differences in average linear acceleration, we might expect that the pulse control scheme would be better at maintaining velocity over successive tail beats. In preliminary experiments we have found the pulse control scheme capable of executing other composite maneuvers observed in live fish including double bend turns (Domenici and Blake 1991, Howe and Astley 2020). In further studies we will test the compound maneuverability of the C-start and offset control scheme with respect to the pulse control scheme.

Maneuverability is an important component of a robot's overall performance. We developed a novel bio-inspired control scheme to generate a wide range of turns, comparing this control scheme to other methods of turning fish robots from the literature. We expected the novel bio-inspired control scheme to perform better than the others, and while it was superior in limiting recoil and maintaining higher average accelerations, it performed worse in total heading change and maximum centripetal acceleration. There are many more permutation of the control schemes than we were able to test, and we could have interpreted and applied the C-start and offset algorithms differently. This experiment shows that total body bending, regardless of algorithm, is important for heading change performance. As fish robots need to perform a wider range of more complex maneuvers, a control scheme that is flexible enough to accommodate a wide range of behaviors will be necessary. We suggest that considering swimming as a combination of individual pulses rather than a continuous sinusoidal function allows for a unified control scheme that can easily switch between behaviors. Further study is needed to compare the performance of our bio-inspired control algorithm with other existing control schemes as maneuvers and transitions between behaviors increase in complexity.

Acknowledgments

The authors thank Liann Cox and the Ocasek Natatorium Lifeguards for giving us access to the pool. As well as the Vargo family, who allowed us to use their pool to shoot video after the COVID 19 pandemic closed the university campus. Derek Jurestovsky, Caleb Dyck, and Amy Howe helped gather data during this time. Peter Niewiarowski provided guidance constructing statistical models.

Data availability statement

The data that support the findings of this study are available upon reasonable request from the authors.

ORCID iDs

Stephen P Howe https://orcid.org/0000-0003-0436-9078
Andrew R Duff https://orcid.org/0000-0002-1489-6624
Henry C Astley https://orcid.org/0000-0003-0136-1433

References

Akanyeti O and Fetherstonhaugh S 2020 A kinematic chain model to quantify undulatory locomotion in animals and robots *Integrative and Comparative Biology* vol 60 (Oxford: Oxford University Press) p E3

Anderson J M and Chhabra N K 2002 Maneuvering and stability performance of a robotic tuna *Integr. Comp. Biol.* **42** 118–26

Bal C, Ozmen Koca G, Korkmaz D, Akpolat Z H and Ay M 2019 CPG-based autonomous swimming control for multi-tasks of a biomimetic robotic fish *Ocean Eng.* **189** 106334

Blevins E and Lauder G V 2013 Swimming near the substrate: a simple robotic model of stingray locomotion *Bioinspiration Biomimetics* **8** 016005

Borazjani I and Sotiropoulos F 2010 On the role of form and kinematics on the hydrodynamics of self-propelled body/caudal fin swimming *J. Exp. Biol.* **213** 89–107

Cen L and Erturk A 2013 Bio-inspired aquatic robotics by untethered piezohydroelastic actuation *Bioinspiration Biomimetics* **8** 016006

Chen D, Wu Z and Yu J 2019 Effect of compliant passive joint on swimming performance for a multi-joint robotic fish *2019 IEEE Int. Conf. on Robotics and Biomimetics*

Chen X, Yu J, Wu Z, Meng Y and Kong S 2018 Toward a maneuverable miniature robotic fish equipped with a novel magnetic actuator system *IEEE Trans. Syst. Man Cybern.* **50** 2327–37

Clark A J, Moore J M, Wang J, Tan X and McKinley P K 2012 Evolutionary design and experimental validation of a flexible caudal fin for robotic fish *Artificial Life Conf. Proc.* vol 12

Coral W, Rossi C, Curet O M and Castro D 2018 Design and assessment of a flexible fish robot actuated by shape memory alloys *Bioinspiration Biomimetics* **13** 056009

Domenici P and Blake R W 1991 The kinematics and performance of the escape response in the angelfish (Pterophyllum Eimekei) *J. Exp. Biol.* **156** 187–205

Ellerby D J, Berlin C G, Cathcart K J, Dornon M K, Feldman A, Gee J K and Moran C J 2018 Assessing the ecological relevance of swimming performance traits: a case study of bluegill sunfish (*Lepomis macrochirus*) *Aquat. Ecol.* **52** 311–22

Epstein M, Colgate J E and MacIver M A 2005 A biologically inspired robotic ribbon fin *Proc. of the IEEE/RSJ Int. Conf. on Intelligent Robots and Systems, Workshop on Morphology, Control, and Passive Dynamics*

Fish F E 2013 Advantages of natural propulsive systems *Mar. Technol. Soc. J.* **47** 37–44

Hirata K, Takimoto T and Tamura K 2000 Study on turning performance of a fish robot *1st Int. Symp. on Aqua Bio-Mechanisms*

Howe S P and Astley H C 2020 The control of routine fish maneuvers: connecting midline kinematics to turn outcomes *J. Exp. Zool.* **333** 579–94

Ijspeert A J 2008 Central pattern generators for locomotion control in animals and robots: a review *Neural Netw.* **21** 642–53

Jayne B C and Lauder G V 1993 Red and white muscle activity and kinematics of the escape response of the bluegill sunfish during swimming *J. Comp. Physiol.* A **173** 495–508

Jian-Xin X and Xue-Lei N 2011 Analytical control design for a biomimetic robotic fish *2011 IEEE Int. Symp. on Industrial Electronics*

Jindong L and Huosheng H 2005 Mimicry of sharp turning behaviours in a robotic fish *Proc. of the 2005 IEEE Int. Conf. on Robotics and Automation*

Yu J, Wang S and Tan M 2003 Basic motion control of a free-swimming biomimetic robot fish *42nd IEEE Int. Conf. on Decision and Control* (IEEE)

Kelasidi E, Pettersen K Y and Gravdahl J T 2014 Stability analysis of underwater snake robot locomotion based on averaging theory *2014 IEEE Int. Conf. on Robotics and Biomimetics*

Lauder G, Akanyeti O, Castro-Santos T, Disanto V, Dong H, Goerig E and Wainwright D 2018 Comparative undulatory kinematics in swimming fishes: quantitative database from a diversity of species *Integrative and Comparative Biology* **58**

Lighthill M J 1960 Note on the swimming of slender fish *J. Fluid Mech.* **9** 305–17

Maladen R D, Ding Y, Umbanhowar P B, Kamor A and Goldman D I 2011 Mechanical models of sandfish locomotion reveal principles of high performance subsurface sand-swimming *J. R. Soc. Interface* **8** 1332–45

McClelland J 1839 *Indian Cyprinidae* 19 (Calcutta: Bishop's College Press)

Ming A, Hashimoto K, Zhao W and Shimojo M 2013 Fundamental analysis for design and control of soft fish robots using piezoelectric fiber composite *2013 IEEE Int. Conf. on Mechatronics and Automation*

Ming A, Ichikawa T, Zhao W and Shimojo M 2014 Development of a sea snake-like underwater robot *2014 IEEE Int. Conf. on Robotics and Biomimetics (ROBIO 2014)*

Morgansen K A, Triplett B I and Klein D J 2007 Geometric methods for modeling and control of free-swimming fin-actuated underwater vehicles *IEEE Trans. Robot.* **23** 1184–99

Neveln I D, Bai Y, Snyder J B, Solberg J R, Curet O M, Lynch K M and MacIver M A 2013 Biomimetic and bio-inspired robotics in electric fish research *J. Exp. Biol.* **216** 2501–14

Niu X and Xu J 2014 Modeling, control and locomotion planning of an anguilliform robotic fish *Unmanned Syst.* **02** 295–321

Ozmen Koca G, Bal C, Korkmaz D, Bingol M, Ay M, Akpolat Z and Yetkin S 2018 Three-dimensional modeling of a robotic fish based on real carp locomotion *Appl. Sci.* **8** 180

Phamduy P, Vazquez M A, Kim C, Mwaffo V, Rizzo A and Porfiri M 2017 Design and characterization of a miniature free-swimming robotic fish based on multi-material 3D printing *Int. J. Intell. Robot. Appl.* **1** 209–23

Pin Y H, Hoe L B, Kin K T T and Saad I 2011 Swimming motion control for biometric fish robot by utilizing turning coefficient *2011 2nd Int. Conf. on Intelligent Systems, Modelling and Simulation*

Ren Q, Xu J, Gao W and Niu X 2012 Generation of robotic fish locomotion through biomimetic learning *2012 IEEE/RSJ Int. Conf. on Intelligent Robots and Systems*

Su Z, Yu J, Tan M and Zhang J 2011 A closed-loop method to generate fast C-start for a robotic fish *2011 IEEE Int. Conf. on Mechatronics and Automation*

Su Z, Yu J, Tan M and Zhang J 2014 Implementing flexible and fast turning maneuvers of a multijoint robotic fish *IEEE/ASME Trans. Mechatronics* **19** 329–38

Tomie M, Takiguchi A, Honda T and Yamasaki J 2005 Turning performance of fish-type microrobot driven by external magnetic field *IEEE Trans. Magn.* **41** 4015–7

Tytell E, Holmes P and Cohen A 2011 Spikes alone do not behavior make: why neuroscience needs biomechanics *Curr. Opin. Neurobiol.* **21** 816–22

Wang M, Dong H, Li X, Zhang Y and Yu J 2019 Control and optimization of a bionic robotic fish through a combination of CPG model and PSO *Neurocomputing* **337** 144–52

Wang M, Yu J and Tan M 2014 CPG-based sensory feedback control for bio-inspired multimodal swimming *Int. J. Adv. Robot. Syst.* **11** 170

Wang M, Yu J, Tan M and Zhang G 2011 A CPG-based sensory feedback control method for robotic fish locomotion *Proc. of the 30th Chinese Control Conf.*

Wang T, Hu Y and Liang J 2013 Learning to swim: a dynamical systems approach to mimicking fish swimming with CPG *Robotica* **31** 361–9

Webb P W and Fairchild A G 2001 Performance and maneuverability of three species of teleostean fishes *Can. J. Zool.* **79** 1866–77

Wu Z, Yu J, Su Z, Tan M and Li Z 2015 Towards an *Esox lucius* inspired multimodal robotic fish *Sci. China Inf. Sci.* **58** 1–13

Xie F, Li Z, Ding Y, Zhong Y and Du R 2020 An experimental study on the fish body flapping patterns by using a biomimetic robot fish *IEEE Robot. Autom. Lett.* **5** 64–71

Xie F, Zhong Y, Du R and Li Z 2019 Central pattern generator (CPG) control of a biomimetic robot fish for multimodal swimming *J. Bionic Eng.* **16** 222–34

Yang Y, Wang J, Wu Z and Yu J 2018 Fault-tolerant control of a CPG-governed robotic fish *Engineering* **4** 861–8

Yu J, Chen S, Wu Z, Chen X and Wang M 2018 Energy analysis of a CPG-controlled miniature robotic fish *J. Bionic Eng.* **15** 260–9

Yu J, Liu L and Wang L 2006 Dynamics and control of turning maneuver for biomimetic robotic fish *2006 IEEE/RSJ Int. Conf. on Intelligent Robots and Systems*

Yu J, Liu L, Wang L, Tan M and Xu D 2008 Turning control of a multilink biomimetic robotic fish *IEEE Trans. Robot.* **24** 201–6

Yu J, Su Z, Wu Z and Tan M 2016 Development of a fast-swimming dolphin robot capable of leaping *IEEE/ASME Trans. Mechatronics* **21** 2307–16

Yu J and Tan M 2020 Implementing flexible and fast turning maneuvers of multijoint robotic fish *Motion Control of Biomimetic Swimming Robots* (Berlin: Springer) pp 47–69

Yu J, Wang L, Shao J and Tan M 2007 Control and coordination of multiple biomimetic robotic fish *IEEE Trans. Control Syst. Technol.* **15** 176–83

Yu J, Wang M, Tan M and Li Y F 2009 Step function based turning maneuvers in biomimetic robotic fish *2009 IEEE Int. Conf. on Robotics and Automation*

Yuan J, Yu J, Wu Z and Tan M 2015 Enhancing swimming performance of a biomimetic robotic fish by optimizing oscillator phase differences of a CPG model *2015 IEEE Int. Conf. on Robotics and Biomimetics*

Zhang S, Qian Y, Liao P, Qin F and Yang J 2016 Design and control of an agile robotic fish with integrative biomimetic mechanisms *IEEE/ASME Trans. Mechatronics* **21** 1846–57

Zhong Y, Li Z and Du R 2017 A novel robot fish with wire-driven active body and compliant tail *IEEE/ASME Trans. Mechatronics* **22** 1633–43

Zhong Y, Li Z and Du R 2018 Robot fish with two-DOF pectoral fins and a wire-driven caudal fin *Adv. Robot.* **32** 25–36